

1 **Major contribution of neutral clusters to new particle**
2 **formation at the interface between the boundary layer and**
3 **the free troposphere**

4
5 **C. Rose¹, K. Sellegri¹, E. Asmi², M. Hervo¹, E. Freney¹, A. Colomb¹, H.**
6 **Junninen³, J. Duplissy³, M. Sipilä³, J. Kontkanen³, K. Lehtipalo^{3,4} and M.**
7 **Kulmala³**

8 [1]{Laboratoire de Météorologie Physique CNRS UMR6016, Observatoire de Physique du
9 Globe de Clermont-Ferrand, Université Blaise Pascal, France}

10 [2]{Finnish Meteorological Institute, P.O. Box 503, 00101 Helsinki, Finland}

11 [3]{Department of Physics, University of Helsinki, Helsinki, Finland}

12 [4] {Airmodus Ltd, Gutaf Hällströmin katu 2, 00560 Helsinki, Finland}

13 Correspondence to: K. Sellegri (k.sellegri@opgc.univ-bpclermont.fr)

14
15 **Abstract**

16 The formation of new aerosol particles in the atmosphere is a key process influencing the
17 aerosol number concentration as well as the climate, in particular at high altitude, where the
18 newly formed particles directly influence cloud formation. However, free tropospheric new
19 particle formation (NPF) is poorly documented due to logistic limitations and complex
20 atmospheric dynamics around high altitude stations that make the observation of this day-time
21 process challenging. Recent improvements in measurement techniques make now possible the
22 detection of neutral clusters down to ~1nm sizes, which opens new horizons in our
23 understanding of the nucleation process. Indeed, only the charged fraction of clusters has been
24 reported in the upper troposphere up to now. Here we report day time concentrations of
25 charged and neutral clusters (1 to 2.5 nm mobility diameter) recorded at the interface between
26 the boundary layer (BL) and the FT as well as in the FT at the altitude site of puy de Dôme
27 (1465m a.s.l.), central France, between 10th and 29th February, 2012. Our findings
28 demonstrate that in the FT, and especially at the interface between the BL and the FT, the

1 formation of 1.5 nm neutral clusters significantly exceeds the one of ionic clusters during
2 NPF events, clearly indicating that they dominate in the nucleation process. We also observe
3 that the total cluster concentration significantly increases during NPF events compared to the
4 other days, which was not clearly observed for the charged cluster population in the past.
5 During the studied period, the nucleation process does not seem to be sulphuric acid-limited
6 and could be promoted by the transport of pollutants to the upper troposphere, coupled with
7 low temperatures.

8

9 **1 Introduction**

10 New particle formation directly impacts the total atmospheric aerosol particle concentration
11 and has an indirect effect on climate through cloud related radiative processes (Makkonen et
12 al., 2012). The formation of aerosol particles has been observed and studied in various
13 environments around the world. It appears that depending on the location, new particle
14 formation (NPF) events do have specificities in term of intensity and space scales, both
15 horizontal (Kulmala et al., 2004) and vertical (Boulon et al., 2011). The formation of new
16 particles in the FT is particularly important as actual global models predict that it contributes
17 to an important fraction of the total atmospheric column aerosol number concentration
18 (Merikanto et al., 2009) and hence potential CCN number concentrations (Spracklen et al.,
19 2008). However, observation of NPF at high altitude is still scarce, especially using the
20 instrumentation adapted to the study of nanometer-sized clusters.

21 Aerosol formation results from a complex sequence of different processes including the
22 production of clusters from gaseous precursors and the growth of these clusters to particles.
23 Despite the fact that instrumentation is continuously improved, our understanding of the
24 aerosol formation mechanism is still limited. Especially challenging tasks are to quantitatively
25 detect neutral clusters and identify the chemical species involved in the first step of the NPF.

26 Until a few years ago, the measurement techniques able to detect the smallest cluster sizes
27 were based on electrostatic methods, such as the NAIS (Neutral Air Ion Spectrometer, Mirme
28 and Mirme, 2013). These methods require artificial charging of neutral particles prior to the
29 measurement. Studies concerning the NAIS sampling technique showed that reliable
30 measurements of neutral cluster concentrations could not be ensured for diameters smaller
31 than ~2 nm because of the post filtering process of corona generated ions (Asmi et al., 2009;
32 Manninen et al., 2011). Recent improvements of condensation techniques make it now

1 possible to measure the concentrations and the size distributions of charged as well as neutral
2 particles down to ~ 1 nm sizes (Kim et al., 2003; Vanhanen et al., 2011; Kuang et al., 2012a).
3 This size limit appears to be more relevant for the study of nucleation compared to the 2 nm
4 size limit of the NAIS since it was recently shown that atmospheric nucleation occurs at a size
5 $1.5 \text{ nm} \pm 0.4 \text{ nm}$ (Kulmala et al., 2007; Kirkby et al., 2011; Kulmala et al., 2013). Using PSM
6 (Particle Size Magnifier, Vanhanen et al., 2011) measurements, Kulmala et al. (2013) have
7 recently reported a high variability, both in term of spatial and temporal scales, of neutral
8 cluster concentrations at boundary layer sites. In Hyytiälä, Finland, they were also able to
9 quantify the fraction of particles produced exclusively by the neutral pathway, i.e. excluding
10 ion – mediated nucleation and recombination of oppositely charged ions (Kontkanen et al.,
11 2013). Several studies performed prior to the development of the PSM have reported that the
12 charged nucleation pathway seemed to be a more favourable route at high altitude compared
13 to boundary layer (BL) stations for the formation of new particles (Boulon et al., 2010;
14 Manninen et al., 2010).

15 In this paper, we report the diurnal variability of total, charged and neutral cluster
16 concentrations as well as NPF event characteristics measured between 10th and 29th February
17 2012 using PSM and NAIS data recorded in clear sky conditions at the puy de Dôme station
18 (7 days available). This period was selected due to the occurrence of very low temperatures in
19 central and Western Europe, that led to unusually low BL height coupled with increased
20 pollution levels. The low BL height permitted the puy de Dôme station to lay in the free
21 troposphere (FT) even during day time, when nucleation occurred, or, more frequently, at the
22 interface between the BL and the FT. Thus, the main purpose of this paper is to investigate
23 cluster formation and concentrations in these unusual conditions, with a special focus on
24 neutral clusters.

25 **2 Measurements and methods**

26 **2.1 Measurement site**

27 Measurements were carried out at the puy de Dôme (PUY) site ($45^{\circ}46'$ N, $2^{\circ}57'$ E) in central
28 France (part of European networks EMEP/GAW/ACTRIS). The station is located at the top of
29 the puy de Dôme mountain (1465 m a.s.l) and is mainly surrounded by fields and forest. The
30 nearest town, Clermont-Ferrand (300 000 inhabitants), is located 16 km East of the mountain
31 at 396 m a.s.l. More detailed description of the station can be found in Freney et al. (2011).

1 **2.2 Instrumentation**

2 **2.2.1 The Neutral cluster and Air Ion Spetromecter (NAIS)**

3 The charged cluster size distributions were recorded with an NAIS (Airel Ltd., Mirme et al.,
4 2007; Mirme and Mirme, 2013) which ensures ion measurement in the mobility range 0.0013
5 $- 3.2 \text{ cm}^2\text{V}^{-1}\text{s}^{-1}$, corresponding to particle Millikan diameters between 0.8 and 42 nm. The
6 instrument was operating on the roof of the station behind an individual non-heated short inlet
7 (30 cm). This setup implies that measurements are directly influenced by cloudy conditions.
8 The AIS sampling method is based on the simultaneous measurement of positively and
9 negatively charged particles with two identical cylindrical Differential Mobility Analysers
10 (DMA). Each analyser uses a sample flow rate of 30 lpm and a sheath flow rate of 60 lpm,
11 which minimizes diffusion losses and ensures significant signal to noise ratio, even in case of
12 low concentrations. The inner cylinder of each DMA is divided into four isolated rings
13 charged with a constant voltage during a measurement cycle. The outer cylinder is made of 21
14 isolated rings connected to 21 electrometers. Naturally charged aerosol particles are moved in
15 the DMA by a radial electric field from the inner cylinder to the outer one. The current carried
16 by ions entering the DMA is amplified and measured with electrometers. After a
17 measurement cycle, the instrument runs an offset measurement in order to estimate the noise
18 of the electrometers. During the offset measurement, all the particles, both neutral and
19 charged, must be removed from the sample air before they enter the DMAs. For that purpose,
20 all the particles are thus charged with a unipolar corona charger and electrically filtered before
21 reaching the DMAs.

22 The NAIS also allows the detection of total particles after a pre-charging process during
23 which particles are charged by ions originating from a corona discharge. The sampling
24 analysis method is then similar to the one described for the ions.

25 **2.2.2 The Particle Size Magnifier (PSM)**

26 The total (neutral + ion) cluster concentrations (N_{tot}) were measured with a PSM (Airmodus
27 A09, Vanhanen et al., 2011) which allows cluster detection down to ~ 1 nm sizes. The PSM is
28 a mixing – type instrument in which the activation of particles is based on a rapid and
29 turbulent mixing of aerosol and heated air saturated with diethylene glycol (DEG). Optical
30 particle counting is done with an ordinary CPC (TSI 3010). The sample flow rate of the PSM
31 is fixed at 2.5 lpm while the saturator flow rate can be varied in the range 0.1 – 1 lpm, which

1 corresponds to varying the 50% activation diameter of the instrument between 1 – 2.5 nm by
2 changing the mixing ratio of the DEG vapor. For the measurements used in this study, the
3 PSM was operating in a scanning mode with 120 steps between saturator flow rates 0.1 – 1
4 lpm and a time resolution of 4 minutes.

5 2.2.3 Atmospheric pressure Interface time of flight mass spectrometer (APi- 6 TOF)

7 In the present study, APi-TOF measurements (Junninen et al., 2010) were not directly used to
8 investigate the cluster composition but rather to modify a proxy for sulfuric acid
9 concentrations at the PUY, as explained in section 2.3.1. The method used to calculate neutral
10 H₂SO₄ concentrations from naturally charged negative ion measurements conducted with the
11 APi-Tof is similar to the one proposed by Eisele (1989). We obtained a calibration coefficient
12 specific to the APi-Tof from the ratio of the sulphuric acid concentration calculated from the
13 APi-Tof naturally charged ion signals to sulphuric acid concentration measured by a
14 calibrated CI-API-TOF (Jokinen et al., 2012). The comparison was achieved during a field
15 campaign that took place in Hyytiälä atmospheric station (Hari and Kulmala, 2005).

16 2.2.4 LIDAR measurements

17 In order to get an estimation of the boundary layer (BL) height, here assumed to be equal to
18 the aerosol mixing layer height, LIDAR measurements were achieved from the roof of the
19 Laboratoire de Météorologie Physique (45°45' N, 3°6' E, 410 m a.s.l.). The LIDAR is a
20 Raymetrics Rayleigh-Mie LIDAR emitting at 355 nm, with both parallel and orthogonal
21 polarization channels. The spatial resolution of the LIDAR is 7.5 m. The instrument provides
22 volume backscatter and extinction profiles, as well as the depolarisation ratio and water
23 vapour mixing ratio. A more complete description of the LIDAR is available in Hervo et al.
24 (2012). The method used for the determination of the BL height is detailed in section 2.3.2.

25 2.2.5 Auxiliary measurements

26 Auxiliary measurements were used to explain the observed NPF and cluster concentration
27 features reported in the present study. Numerous atmospheric parameters such as global
28 radiation, wind speed and direction, temperature, pressure and relative humidity (*RH*) as
29 well as atmospheric trace gases (including *SO*₂, CO and NO₂) and particulate black carbon
30 (*BC*) are continuously recorded at the station. *SO*₂ measurements were performed using a

1 low level SO_2 analyser (pulsed fluorescence TEI 43CTL) while BC measurements were
2 achieved with a Multi Angle Absorption Photometer (MAAP 5012, central wavelength at 637
3 nm). The aerosol particle number size distributions were measured with a custom built
4 Scanning Mobility Particle Sizer (SMPS) operating in the size range 10 – 420 nm. The SMPS,
5 as well as the PSM, were operating behind a Whole Air Inlet (WAI) with a cut-off size of 30
6 μm . More detailed explanations on the SMPS and the inlet system can be found in Venzac et
7 al. (2009). Since clusters were previously shown to be very sensitive to the presence of clouds
8 at high altitude stations (Lihavainen et al., 2007; Venzac et al., 2007), cloudy conditions were
9 filtered out by using RH data. Indeed, cluster ions, and eventually cluster particles, are very
10 efficiently scavenged by the cloud droplets that offer a large condensational sink. Cluster
11 formation and subsequent growth to larger particle sizes would be difficult to follow due to
12 this very high sink. The threshold value $RH = 98\%$ was used to separate in-cloud and out-of-
13 cloud conditions.

14 **2.3 Data analysis**

15 **2.3.1 Sulphuric Acid concentration**

16 Sulphuric acid concentrations ($[H_2SO_4]$) were calculated using a proxy adjusted on
17 concentrations derived from Api-Tof measurements conducted between 30 January and 6
18 February 2012 at the PUY (no data available between 10 and 29 February), during which
19 atmospheric conditions, and especially temperatures, were similar to the conditions observed
20 between 10 and 29 February:

$$21 \quad [H_2SO_4] = k \frac{GlobRad [SO_2]}{CS * RH} \quad (1)$$

22 where k is a scaling factor, and $GlobRad$ is the global radiation in $W\ m^{-2}$, $[SO_2]$ is the
23 sulphur dioxide concentration in $\text{molec}\ cm^{-3}$, CS is the condensation sink in s^{-1} and RH is the
24 relative humidity. The form of Equation (1) was suggested by Mikkonen et al. (2011) and is
25 based on previous work by Petäjä et al. (2009). This proxy was constructed for radiations
26 higher than $10\ W\ m^{-2}$ but the predictive ability is significantly raised for radiations exceeding

1 50 W m^{-2} , which was roughly achieved between 7:30 and 16:30 UTC (- 1h local time in
2 winter) during the studied period. As previously mentioned, in the present study, the scaling
3 factor $k = 6.0060 \times 10^{-7} \text{ m}^2 \text{ W}^{-1} \text{ s}^{-1}$ was empirically obtained by using a linear fitting
4 procedure on sulphuric acid concentrations derived from Api-Tof measurements. After
5 adjusting the proxy, the average positive and negative bias between proxy estimations and the
6 Api-Tof derived concentrations were 0.57×10^7 and $-0.97 \times 10^7 \text{ cm}^{-3}$, respectively.

7 A potential systematic error on the sulfuric acid concentration calculation from the Api-Tof
8 due to a unadapted use of the PUY scaling factor is of course possible, and would affect the
9 absolute values of calculated sulfuric acid concentrations, but not their variability. We thus
10 clearly believe that the accuracy of the proxy derived from Equation (1) and adjusted on
11 measurements is high enough to study the relative changes in the sulfuric acid concentration
12 from one period to the other.

13 2.3.2 Boundary layer height determination

14 The estimation of the BL height was derived from LIDAR data and is based on the fact that
15 aerosol concentrations, and thus the LIDAR signal, show a sudden drop between the BL and
16 the FT. The most common used methods are 1) the measurement of the LIDAR signal
17 variance, 2) the measurement of the LIDAR signal gradient and 3) the analysis of the analogy
18 between the LIDAR signal and a wavelet. The last method, called wavelet covariance
19 technique (WCT), appears to be the most relevant (Baars et al., 2008) and was used in the
20 present study. The WCT uses the covariance transform W of the Haar function h (Brooks,
21 2003):

$$22 \quad W(a, b) = \frac{1}{a} \int_{z_b}^{z_t} S(z) h\left(\frac{z-b}{a}\right) dz \quad (2)$$

23 with

$$h\left(\frac{z-b}{a}\right) = \begin{cases} 1: b - \frac{a}{2} \leq z \leq b \\ -1: b \leq z \leq b + \frac{a}{2} \\ 0: elsewhere \end{cases} \quad (3)$$

where z is altitude, $S(z)$ is the LIDAR backscatter profile corrected with z^2 , z_b and z_t are the lower and upper limit of the profile, respectively, b is the altitude at which the Haar function is centred and a is the spatial extent. a was set to $12 \Delta r$ according to Baars et al. (2008), where $\Delta r = 7.5$ m is the spatial resolution of the LIDAR.

Equation (3) was applied to all LIDAR profiles with a time resolution of 10 minutes and for each profile the BL height was identified as the maximum of the W function. These calculations were made under the assumptions that 1) topography does not influence the BL height at the location where the LIDAR measurements take place and 2) aerosol particles are homogeneously mixed within the BL.

LIDAR measurements were previously used by Boulon et al. (2011) to derive BL height at the PUY, but with a calculation method which slightly differs from the WCT. In fact, the WCT aims at finding the upper limit of the aerosol layer, whereas the method developed by Boulon et al. (2011) was designed to find the transition between Mie and Rayleigh diffusion regimes. When applying this last method to our dataset, we find BL heights that are very similar to those derived from the WCT, i.e. 8% higher on average. The reliability of the LIDAR derived BL height was also tested and approved by Boulon et al. (2011) using potential equivalent temperature.

2.3.3 Particle formation and growth rate calculations

Particle formation and growth rates are key entities to characterize a NPF event, especially in the very first steps of the formation process, i.e. between 1 and 3 nm. As previously mentioned, the PSM was measuring in a scanning mode during the studied period, but the differences between the concentrations of the successive size classes were too small to allow determination of size distributions, and hence any growth rate calculation. Thus we calculated the total particle formation rate at 1.5 nm, $J_{1.5}^{tot}$, from the total particle concentration measured in the size range 1-2.5 nm by the PSM, $N_{1-2.5}$, and by using the growth rates derived from the

1 NAIS in the ion mode in the size range 1.5-3 nm, $GR_{1.5-3}$. GRs were calculated with the
 2 “maximum concentration” method originating from Hirsikko et al. (2005). In this method, the
 3 time corresponding to the maximum concentration in each size class of the selected size range
 4 is first determined by fitting a normal distribution to the size class concentration; the growth
 5 rate of the corresponding size range is then obtained by a linear least square fit through the
 6 time values previously found. The total particle formation rate at 1.5 nm was finally
 7 calculated according to Eq. (4), from Kulmala et al. (2007):

$$8 \quad J_{1.5}^{tot} = \frac{dN_{1-2.5}}{dt} + CoagS_{1.5} \times N_{1-2.5} + \frac{1}{1.5nm} GR_{1.5-3} \times N_{1-2.5} \quad (4)$$

9 where $CoagS_{1.5}$ represents the loss of 1.5 nm particles on larger pre-existing particles from
 10 the background size distribution. In the case of charged particles, Eq. (4) is completed by two
 11 terms to take into account the loss of ions by recombination and the attachment of ions to
 12 neutral particles:

$$13 \quad J_{1.5}^{\pm} = \frac{dN_{1-2.5}^{\pm}}{dt} + CoagS_{1.5} \times N_{1-2.5}^{\pm} + \frac{1}{1.5nm} GR_{1.5-3} \times N_{1-2.5}^{\pm} + \alpha \times N_{1-2.5}^{\pm} N_{<2.5}^{\mp} - \beta \times N_{1-2.5} N_{<1}^{\pm} \quad (5)$$

14 where $N_{1-2.5}^{\pm}$ is the ion number concentration (positive or negative) in diameter range 1-2.5
 15 nm and $N_{<y}^{\pm}$ is the ion concentration below y nm. α and β are the ion-ion recombination
 16 and the ion-neutral attachment coefficient, respectively, and were assumed to be equal to 1.6
 17 $\times 10^{-6} \text{ cm}^3 \text{ s}^{-1}$ and $0.01 \times 10^{-6} \text{ cm}^3 \text{ s}^{-1}$, respectively (Tamm et al. 2005).

1 **3 The smallest particles include both clusters and large molecules, and the**
2 **exact critical size cannot be known (Kulmala et al., 2013). For that reason,**
3 **and also to investigate the evolution of the formation rate as a function of**
4 **cluster size, particle formation rates are usually calculated for different size**
5 **classes. The formation of 3 nm clusters (J_3^{tot}) and ions (J_3^\pm) was thus**
6 **analysed by using the cluster concentrations in the size range 3-5 nm and**
7 **the growth rate over the 3-5 nm diameter range, both derived from NAIS**
8 **measurements. Results and discussion**

9 **3.1 Charged and neutral cluster concentrations in the free troposphere**

10 **3.1.1 Identification of free tropospheric conditions**

11 The present study includes seven days between the 10th and the 29th of February 2012. Based
12 on a visual analysis of the contour plot of the ion size distribution, five of these days were
13 classified as NPF event days (10th, 11th, 12th, 28th and 29th of February) and the remaining two
14 (21st and 22nd of February) were considered as non-event days. These days were selected
15 because they were characterized by clear skies and they gave a unique chance to investigate
16 free tropospheric conditions and the interface between the BL and the FT during the first part
17 of the day, i.e. when nucleation and early growth of new particles occur. Such conditions at
18 the station can only be achieved when convective air mass movements are limited. These
19 criteria were fulfilled during a period of exceptionally cold temperatures during winter 2012
20 in Europe. In the following, the studied dataset will be divided into three sub-periods, so that
21 the 10th, 11th and 12th will be referred as “Period 1”, 21st and 22nd as “Period 2” and 28th and
22 29th as “Period 3”.

23 Figure 1 shows the BL height derived from LIDAR measurements using the WCT method
24 (see section 2.3.2). SMPS particle size distributions (PSD), nitrogen dioxide concentrations
25 (NO₂) and wind speed are given as additional information to distinguish between FT and BL
26 on Fig. 2.

27 During Periods 2 and 3, the BL height rarely exceeds the altitude of the PUY, indicating that
28 the station could be almost continuously above the BL (Fig. 1). However, NO₂ concentration
29 starts to increase between 10:30 and 11:00 (UTC, -1h local time in winter) on the 28th and
30 29th, which coincide with the detection of an accumulation mode on the PSD (Fig 2). These

1 last observations lead to balance LIDAR indications and suggest that during Period 3, the
2 measurement site could be located in the FT in the early morning until ~ 10h30, and is then
3 progressively influenced by the upper BL. A closer look at the 28th reveals that the total
4 cluster concentration starts to increase around 10:00, i.e. before NO₂ and others BL tracers,
5 such as the relative humidity and the condensation sink (Fig. 3), and reaches its maximum at
6 11:45, which suggests that the nucleation process could be initiated in the FT, and then
7 continued in the interface layer between the BL and the FT. In contrast, on the 29th (figure not
8 shown), the beginning of the major cluster concentration increase is seen at 11:30, i.e. almost
9 one hour after the beginning of the NO₂ augmentation. Thus it is likely that contrary to the
10 28th, on this last day of Period 3 the nucleation process is most probably triggered at the
11 interface between the BL and the FT rather than in the FT. On the 21st, based on LIDAR
12 measurements and PSD, it is likely that the station is located in the BL in early morning and
13 late evening, i.e. outside of the nucleation hours, and in the FT during the rest of the day. On
14 the 22nd, all measurements agree to conclude that the station is in the FT during the whole
15 day.

16 On the contrary, during Period 1 the BL height displays a clear diurnal variation with a
17 maximum between 1700 and 2000 m a.s.l. around 17:00 UTC (- 1h local time in winter).
18 LIDAR measurements suggest that during these days, the PUY could be in the FT until 12:00
19 UTC and then progressively reached by the BL in the afternoon (Fig. 1). However, on the 10th
20 and the 11th, considering the presence of a significant accumulation mode on the PSD
21 (missing data on the 10th are due to an instrument failure), the high NO₂ concentrations and
22 the higher variability of wind speed (Fig. 2), it is likely that in the morning, the station is not
23 in the FT but rather at the interface between the BL and the FT. The fact that NO₂
24 concentrations show higher values compared to Period 3 suggests that on the 10th and 11th,
25 nucleation hours are most probably characterized by interface/upper BL conditions, whereas
26 interface/FT conditions were found to be predominant on the 28th and 29th. On the 12th, NO₂
27 concentrations are slightly decreased compared to the previous days, and the accumulation
28 mode also seems to be less intense. These conditions are very similar to the conditions
29 observed during Period 3, suggesting that during the nucleation hours, the station could be in
30 the upper part of the interface layer between the BL and the FT, almost in the FT.

31 In short, during the selected days, nucleation hours at the station are characterized by upper
32 BL/interface conditions during Period 1, free tropospheric conditions during Period 2 and

1 interface/FT conditions during Period 3, allowing a direct comparison of the events occurring
2 in the different conditions and an investigation of the parameters playing a key role during the
3 different sub-periods.

4 Previous observations of cluster and aerosol size distributions at high altitudes have rarely
5 shown NPF events occurring in the FT. NPF events at high altitudes were always observed to
6 occur during upwind valley winds (Venzac et al., 2008), or very close to the interface between
7 the BL and the FT (Boulon et al., 2011). The present observations from Period 3, and more
8 especially from the 28th are hence one of the first showing NPF in the FT during clear sky
9 conditions.

10 3.1.2 Charged and neutral cluster concentrations

11 We measured total (N_{tot}) and charged (N_i) cluster concentrations in the range 1-2.5 nm
12 mobility diameter, using respectively the PSM and the NAIS. The neutral cluster
13 concentrations (N_n) in the same size range were calculated according to $N_n = N_{tot} - N_i$. Fig.
14 4 shows the mean diurnal variation of total and charged cluster concentrations, separately for
15 the three sub-periods. In agreement with previous observations at the site (Manninen et al.,
16 2009; Boulon et al., 2011; Rose et al., 2013) cluster ions appear to be present on both event
17 and non-event days. Charged cluster concentrations are on average higher during Periods 2
18 and 3, when the station is more frequently disconnected from the BL compared to Period 1
19 (factor 1.5 between Periods 1 and 3). Charged cluster concentrations do not show any clear
20 diurnal variations, with the exception of the positive cluster ions which exhibit higher
21 concentrations around 12:00 UTC during Period 1. This observation is supported by the
22 values reported in Table 1: the median concentration calculated from the nucleation hours
23 (10:30 – 14:00 UTC) is increased by a factor 1.72 compared to the median calculated over the
24 whole day during Period 1. This behaviour of positive ions was previously observed by Rose
25 et al. (2013), who reported that positive cluster ion concentrations were increased during NPF
26 events over a five years long study. The contrasting behaviour of positive ions observed
27 during Period 3 might be explained by the unusual atmospheric conditions - especially low
28 temperatures and free tropospheric conditions (Fig. 1, 2, 4a). Positive cluster ion
29 concentrations always exceed negative cluster concentrations, especially during Period 2
30 (factor 3.23). This trend differs from the results of the long-term study by Rose et al.(2013)

1 and might again be eventually explained by the atmospheric conditions observed in February
2 2012.

3 In contrast with the behaviour of cluster ions, the total cluster concentration displays very
4 different trends and values on event days compared to non-event days (Fig. 3). On non-event
5 days, the total cluster concentration does not significantly vary with the time of the day and is
6 almost continuously below the cluster ion concentration. This last observation supports the
7 fact that the PSM could be unable to detect all of the cluster ions, most likely because of their
8 chemical composition (Kangasluoma et al., 2013; Wimmer et al., 2013). In the present study,
9 we observed that for ion concentrations below $\sim 500 \text{ cm}^{-3}$, the total cluster concentration
10 measured by the PSM was systematically lower than the ion concentration, leading to non-
11 physical negative values for the neutral cluster concentration. There is no correction for this
12 artefact, as it depends on the chemical composition of the clusters, which is unknown during
13 nucleation events. In order to remain physically correct but avoid overestimating the total
14 cluster concentration, we decided to introduce a lower detection limit (LDL) of 500 cm^{-3} for
15 total cluster concentrations and to filter out all the total cluster concentrations that were below
16 this limit. Hence, the total cluster concentrations that we report in this work are a lower limit
17 of the actual total cluster concentrations.

18 On event days, the total cluster concentration exhibits a very clear diurnal variation with a
19 maximum detected between 10:30 and 14:00 UTC. One should note that these maxima
20 significantly vary from day to day, since the median total cluster concentration calculated
21 during the nucleation hours of Period 1 is more than doubled compared to Period 3 (Table 1).
22 This last observation is mainly explained by the low concentrations observed on the 28th,
23 during which nucleation hours were most probably characterized by interface/FT conditions,
24 suggesting that the formation of neutral clusters could be less intense in the FT compared to
25 interface/BL conditions. This last point will be further discussed in the next sections.

26 The observed diurnal variation of the cluster concentration can be explained by the formation
27 of clusters during the nucleation process in the morning and their growth and/or removal on
28 pre-existing particles in the afternoon. During the nucleation hours, the total cluster
29 concentration more frequently exceeds the charged cluster concentration, clearly indicating
30 the formation of neutral clusters. In particular, averaged neutral cluster concentrations exceed
31 the charged cluster concentration by a factor 4.3 during Period 1, and the charged fraction
32 $f = N_i/N_{tot}$ is close to 0.23 during the nucleation peak. During Period 3, neutral clusters are

1 also clearly increased during the nucleation process, but the charged fraction is significantly
2 higher compared to Period 1 (0.78), suggesting again that the efficiency of neutral pathways
3 could be less important when free tropospheric conditions are predominant. Outside of the
4 nucleation hours, total cluster concentrations are below the charged cluster concentration,
5 being very similar to the concentrations recorded on non-event days during Period 2.

6 The continuous presence of cluster ions has already been reported by several studies at ground
7 stations, both at low (Manninen et al., 2009) and at high altitude (Boulon et al., 2010; Rose et
8 al., 2013) and the diurnal variation of the charged cluster concentration on event days was
9 also observed at several stations (Hörrak et al., 2008; Boulon et al., 2010; Rose et al., 2013).
10 According to recent studies, neutral clusters also seem to be ubiquitous in the atmosphere
11 (Lehtipalo et al., 2009; 2010). In their paper, Kulmala et al. (2013) reported a continuous
12 presence of sub-2.1 nm neutral clusters in Hyytiälä, Finland, with concentrations in the range
13 $500 - 20\,000\text{ cm}^{-3}$. In Finokalia, Greece, sub-2.5 nm total cluster concentrations were in the
14 range $10 - 10\,000\text{ cm}^{-3}$, with lower values at night. NAIS airborne measurements from the
15 whole tropospheric column (up to 12 km) conducted in the frame of the EUCAARI –
16 LONGREX campaign (May 2008) were reported by Mirme et al. (2010) and showed similar
17 results. In fact, charged clusters were continuously detected at all altitudes with a mode
18 centred around 1 nm. Between 2.5 and 3 nm, total cluster concentrations significantly
19 exceeded charged concentrations, suggesting a continuous pool of sub -3nm neutral clusters
20 throughout the whole tropospheric column.

21 The observations reported in this section suggest that at the PUY, differences between the
22 charged and total cluster concentrations are significant enough to conclude that, the formation
23 of neutral clusters dominates the formation of total clusters during NPF events occurring at
24 the interface between the BL and the FT, as well as in the FT. Contrarily to airborne
25 measurements, high altitude ground based measurement offer the possibility to study particle
26 formation and growth rates.

27 3.1.3 Particle formation and growth rates

28 Particle formation and growth rates are given in Table 2 for each event day. The formation
29 rates exhibit significant variations from one event to the other. One can notice that the
30 charged formation rates of positive 1.5 nm clusters are significantly higher than the charged
31 formation rates of negative 1.5 nm clusters, and that the difference is more pronounced during

1 Period 3 (factor 6.8 compared to 2.4 during Period 1). Similar observations were reported in
2 the CLOUD (Cosmics Leaving Outdoor Droplets) experiment (Kirkby et al., 2011), which
3 studied the role of sulphuric acid, ammonia and ions in the nucleation process. In particular,
4 the occurrence of ternary nucleation involving sulphuric acid at high ammonia mixing ratios,
5 with typical path on positive way, could explain the excess of positive ions, at least on event
6 days. Moreover, the average formation rates of total 1.5 nm particles exceeds those of charged
7 particles, especially during Period 1 which displays ion induced nucleation fractions (IIN)
8 lower than 4.3% ($J_{1.5}^{tot} \approx 37 \times J_{1.5}^+$ and $J_{1.5}^{tot} \approx 77 \times J_{1.5}^-$), which is relatively low compared to the
9 average values reported for altitude sites (Boulon et al., 2010; Manninen et al., 2010), and
10 especially for the PUY ($12.5 \pm 2.0\%$, Boulon et al., 2011). In contrast, the IIN rates are higher
11 during Period 3, with a value close to 50% on the 28th of February, suggesting that charged
12 pathways could be promoted in the FT compared to the interface between the BL and the FT.
13 However, besides the height of the BL itself, atmospheric parameters such as temperature and
14 relative humidity display significant variations between the different periods, and could also
15 explain the previous observations (Table 3 and Fig. 5). This potential effect is further
16 discussed in Section 3.2.4.

17 In can be seen from Table 2 that the formation rates of charged and neutral 3 nm particles are
18 significantly decreased compared to the formation rates of charged and neutral 1.5 nm
19 clusters, which is due to the loss of small particles by coagulation on bigger pre-existing
20 particles during their growth.

21 *GR* values also experience significant variations between the different events, with a
22 maximum to minimum ratio of 8.7 for $GR_{1.5-3}$ and 4.3 for GR_{3-5} . Particularly, on the 12th and
23 the 29th, which correspond to the strongest particle formation events of the two sub-periods,
24 $GR_{1.5-3}$ displays values larger than 10 nm h^{-1} . In contrast with the particle formation rate, the
25 particle growth rate is on average increasing as function of particle size (Table 2), suggesting
26 the participation of other vapours than sulphuric acid (Kuang et al., 2012b; Kulmala et al.,
27 2013).

28 The results we obtain clearly suggest that in the FT, and even more at the interface between
29 the BL and the FT, the formation of neutral clusters dominates the formation of total clusters
30 during NPF events. This observation goes in the same direction as Lehtipalo et al. (2010) and
31 Kulmala et al. (2013) who observed a very small contribution of ions in the dynamics of sub-

1 2 nm clusters during the nucleation process at the BL site of Hyytiälä. Indeed, both the
2 concentrations of sub- 2 nm clusters and the formation rate of 1.5 nm clusters were found to
3 be clearly dominated by neutral particles, sometimes with differences exceeding several
4 orders of magnitude. $J_{1.5}^{tot}$ values reported for Hyytiälä are similar to the values obtained at the
5 PUY, with maximum values around $5 \text{ cm}^{-3} \text{ s}^{-1}$ at 12:00 UTC. On the contrary, $J_{1.5}^{\pm}$ exhibits
6 slightly lower values in Hyytiälä, being in the range $3 \times 10^{-2} - 6 \times 10^{-2} \text{ cm}^{-3} \text{ s}^{-1}$. This observation
7 is in agreement with the previous observations by Boulon et al. (2010) and Manninen et al.
8 (2010) who suggested that charged nucleation pathways could be promoted at higher altitudes
9 compared to low altitudes.

10 The purpose of the following section is now to investigate the atmospheric conditions that
11 could favour the occurrence of NPF observed during the different periods and their link to
12 cluster concentrations.

13 **3.2 Analysis of the atmospheric conditions promoting particle formation at** 14 **the BL/FT interface and in the FT**

15 As previously mentioned, among the seven studied days, five were identified as event days
16 and the remaining two as non-event days. We further investigated the changes in atmospheric
17 conditions which lead or not to NPF during this period. For this purpose, several parameters
18 were analysed in addition to BL height, including temperature, relative humidity, black
19 carbon concentration, carbon monoxide concentration (CO), as well as condensation sink
20 (CS) and sulphuric acid concentration (H_2SO_4), and are presented in Table 3 and Fig. 5.
21 Three days air mass back trajectories (calculated from the HYSPLIT transport and dispersion
22 mode, Draxler and Rolph, 2003) are also shown in Fig. 6.

23 **3.2.1 Description of the atmospheric conditions in each sub-period**

24 As previously mentioned, during Period 1 the PUY was most probably located at the
25 interface/upper BL in the morning and in the BL during the second part of the day (Fig. 1 and
26 2). Consequently, Period 1 is characterized by high RH (on average 90.8%) (Fig. 5b and
27 Table 3) and displays the highest BC and CO concentrations, with average values of 687.53
28 ng m^{-3} and 210.78 ppb, respectively (Fig. 5c and d). This relatively high level of pollution for
29 the site might in addition also be explained by air masses coming from Eastern Europe,
30 especially on the 11th (Fig. 6). High emissions can originate from biomass and fuel burning

1 from intensive domestic heating due to very cold temperatures occurring during this period,
2 which never exceed -12°C at the PUY, being on average -14.2°C (Fig. 5a). The condensation
3 sink is logically well correlated with *BC* concentrations and displays the highest average
4 value ($1.36 \times 10^{-2} \text{ s}^{-1}$) of the three sub-periods (Fig. 5e). On the contrary, sulphuric acid
5 concentrations are the lowest of the entire measurement period, with an average value of 0.72
6 $\times 10^7 \text{ molec cm}^{-3}$ (Fig. 5f).

7 During Period 2, the BL height rarely reaches the altitude of the station, suggesting that the
8 PUY is hardly influenced by BL direct emissions (Fig. 1 and 2). As a consequence, average
9 *RH* is decreased to 29.3% and *BC* and CO concentrations are also significantly lower
10 compared to Period 1, with typical values in the range $70 - 420 \text{ ng m}^{-3}$ and $100 - 158 \text{ ppb}$,
11 respectively (Fig. 5c and d). Beside the lower altitude of the BL height relative to the site,
12 these lower concentrations may be partly attributed to the geographical origin of air masses
13 reaching the PUY that have turned from Northern Europe sector (Fig. 6), and which have
14 already been reported to be less polluted than Eastern air masses (Venzac et al., 2009;
15 Bourcier et al., 2012). At last, temperatures are higher during Period 2 compared to Period 1
16 (Fig. 5a), which may also lead to less domestic heating and thus lower pollution originating
17 from combustion processes. Consequently, we observe that the condensation sink is also
18 decreased and displays the lowest values of the whole studied period, being on average 1.60
19 $\times 10^{-3} \text{ s}^{-1}$ (Fig. 5e). At the same time, sulphuric acid concentrations are increased compared to
20 Period 1, being the highest of the three sub-periods (Fig. 5f).

21 The last period, referred as “Period 3”, includes the 28th and 29th of February. Period 3 is
22 characterized by the same BL heights as Period 2 (Fig. 1 and 2) but both *RH*, CO
23 concentrations and *CS* (no information concerning *BC* concentrations because of instrument
24 failure) are slightly higher than during Period 2, with average values of 51.8%, $2.4 \times 10^{-3} \text{ s}^{-1}$
25 and 119.86 ppb, respectively (Table 3). Nonetheless, it is worth to note that they remain
26 broadly lower than during Period 1. During Period 3 temperatures continue to increase, so that
27 the contribution of combustion sources to the condensation sink is likely further decreased
28 (Fig. 5a). However, during Period 3, air masses originate from the North – East part of Europe
29 and they cross United Kingdom Islands before reaching the PUY (Fig 6). Thus they are more
30 polluted than the air masses arriving during Period 2. Sulphuric acid concentrations appear to
31 be significantly lower than during Period 2, with an average value of $2.79 \times 10^7 \text{ molec cm}^{-3}$
32 (Fig. 5f).

1 3.2.2 The role of sulphuric acid

2 Based on Fig. 5, Tables 1 and 3, we can first assert that H₂SO₄ is not the main driver of the
3 nucleation process at the PUY, neither at the interface between the BL and the FT nor in the
4 FT. Indeed, despite the fact that Period 2 is characterized by the highest sulphuric acid
5 concentrations, no NPF events were detected during these days. It is worth to note that
6 similar conclusions are obtained when using proxies for the sulphuric acid concentration that
7 includes scaling factors from the literature, such as the ones proposed in Petäjä et al. (2009) or
8 Mikkonen et al. (2011).

9 Also, there is no clear correlation between cluster concentrations and sulphuric acid, as
10 illustrated by Fig. 7a. Especially, sulphuric acid concentrations obtained during Period 1 are
11 on average 3.9 times lower than during Period 3, whereas median neutral cluster
12 concentration is almost 10 times higher during nucleation hours of Period 1. This observation
13 supports the analysis of Boulon et al. (2010, 2011) who reported that at high altitude stations
14 such as the PUY and the Jungfraujoch, Switzerland, gaseous precursors other than sulphuric
15 acid were also involved in the formation and early growth of the clusters into new particles.

16 3.2.3 Influence of the condensation sink

17 The second important result highlighted by Tables 1-3 is that the occurrence of NPF does not
18 seem to be limited by the condensation sink. In fact, NPF is triggered during Periods 1 and 3,
19 which display CS values significantly higher compared to Period 2. This observation
20 contradicts the previous result by Boulon et al. (2011) at the PUY for ionic clusters but
21 supports the results reported at the Jungfraujoch station (Boulon et al., 2010). However, based
22 on Fig. 7b, we observe that while cluster concentrations are not deeply impacted by the CS up
23 to $\sim 7 \times 10^{-3} \text{ s}^{-1}$, they seem to decrease with an increasing CS above this threshold value,
24 suggesting that high CS values do not inhibit the nucleation process but could limit the
25 number of nucleated clusters.

26 In the present study it is likely that condensable compounds involved in the NPF process and
27 condensation sink share the same origin. Gaseous precursors other than sulphuric acid could
28 be oxidized volatile organic compounds, as suggested by several studies (Metzger et al., 2010;
29 Paasonen et al., 2010; Wang and Wexler, 2013). This would explain the fact that during
30 Period 2, which is characterized by dominant free tropospheric conditions and lowest
31 condensation sinks, particle formation is not triggered because of a lack of other gaseous

1 precursors. Thus, our observations suggest that particle formation occurs when the pool of
2 gaseous precursors is supplied to the upper troposphere by inputs of more polluted air masses
3 from the BL. Thus, it is likely that in the lower part of the interface between the BL and the
4 FT (Period 1), particle formation, and especially neutral pathways, are enhanced compared to
5 Period 3 (upper interface layer/FT) thanks to increased amount of gaseous precursors directly
6 coming from the BL. Similar observations were reported by Neitola et al. (2011) at a high
7 altitude Indian Himalayan site (2180m a.s.l.).

8 3.2.4 A potential additional effect of temperature and relative humidity?

9 In the present study, the occurrence of nucleation and the concentration of nucleated clusters
10 have been discussed so far in terms of sulfuric acid concentration and condensation sink only.
11 However, temperature and relative humidity display significant variations in the course of the
12 measurement period and were previously reported in the literature to have effect on the
13 occurrence of nucleation and on the characteristics of the events (formation rates, cluster
14 concentrations). In fact, low temperatures could favor nucleation, and could in particular
15 explain, together with low CS, the occurrence of NPF in the FT and in the low stratosphere
16 (Young et al., 2007). In contrast, the role of the RH appears to be more equivocal. Numerous
17 observations suggest that nucleation could be favored at low RH (e.g.: Birmili et al., 2003)
18 and both the cluster formation rates (Sihto et al., 2006) and the concentration of freshly
19 formed particles (Jeong et al., 2004) were already reported to be anticorrelated with RH.
20 Nonetheless, NPF events were observed in the vicinity of clouds, where RH often exceeds
21 90% (Clarke et al., 1998). In a more recent study based on model simulations, Hamed et al.
22 (2011) suggest that high RH impact the amount of solar radiation, and thus the source of
23 condensable species, rather than the sink term.

24 Thus, it is likely that at the PUY, the very low temperatures measured during Period 1
25 (average -14.24 °C) could explain, at least partly, the occurrence of nucleation, and maybe the
26 intensive formation of neutral clusters compared to Period 3. However, regarding previous
27 observations from the literature, one could have expected less intense NPF events since high
28 RH were simultaneously recorded during Period 1 (90.8%). The opposite trend is observed
29 for the second NPF period, Period 3, which displays increased temperatures (4.96 °C) and
30 decreased RH (51.8 %) compared to Period 1. During Period 2, RH is further decreased (29.3
31 %) and temperatures remain low (-1.40 °C), but despite these conditions, which should, on a
32 first approach, be favorable to nucleation, no event is detected.

1 The previous observations suggest that atmospheric parameters, including temperature, RH,
2 but also sources and sinks, cannot be considered separately. This might be explained by the
3 fact that their effects combine with each other, but the amount of data used in the present
4 study seems to be too small to analyze such combinations or to disentangle the effects of all
5 parameters unambiguously.

6 **4 Conclusion**

7 We investigated the charged and neutral cluster concentrations (1 – 2.5 nm) during NPF
8 events observed to occur at the interface between the BL and the FT and in the FT at the PUY
9 station, during a period characterized by very low temperatures in Europe.

10 Cluster ions were always present and their concentrations did not exhibit any clear diurnal
11 variation. On the contrary, on event days, the total cluster concentrations clearly peaked
12 between 10:30 and 14:00 (UTC), with on average higher concentrations during Period 1
13 (interface/upper BL) than during Period 3 (interface/FT). Total and charged formation rates at
14 1.5 nm ($J_{1.5}^{tot}$ and $J_{1.5}^{\pm}$ respectively) were derived from PSM and NAIS respectively. The
15 formation rate of positive clusters was higher than the one of negative clusters, especially
16 during Period 3. $J_{1.5}^{tot}$ significantly exceeded $J_{1.5}^{\pm}$, particularly during Period 1, suggesting that
17 neutral clusters were clearly driving the first steps of the NPF process at the PUY in the FT,
18 and even more at the interface between the BL and the FT.

19 When investigating the atmospheric conditions promoting nucleation during the studied
20 period, we found that sulphuric acid was not the main species driving the nucleation and early
21 growth process since there was no clear link between sulphuric acid and the cluster
22 concentrations, nor between sulphuric acid and the occurrence of NPF. The increasing growth
23 rate of clusters with size supports the observation of sulphuric acid not being the only
24 contributor to early particle growth. At last, NPF events were detected when the highest
25 condensation sinks were obtained, during Period 1 when the station was in the lower part of
26 the interface between the BL and the FT, suggesting that gaseous precursors other than
27 sulphuric acid could share the same origin as the condensation sink. According to our
28 observations, it is likely that in the upper troposphere, particle formation would be favored
29 when the amount of gaseous precursors available for nucleation and early growth is supplied
30 by inputs of more polluted air masses. Temperature and RH might also influence the

1 occurrence of nucleation but the studied dataset seems to be too small to distinguish between
2 the effects of the different parameters.

3 **Acknowledgement**

4 Support was provided by AXA, Actris, project SOERE ORAURE, ACI-AMS, the Academy
5 of Finland Center of Excellence program (project no. 1118615), ERC-Advanced
6 "ATMNUCLE" grant no. 227463), CRAICC and the Nordic Center of Excellence CRAICC.

7 **References**

8 Asmi, E., Sipilä, M., Manninen, H. E., Vanhanen, J., Lehtipalo, K., Gagné, S., Neitola, K.,
9 Mirme, A., Mirme, S., Tamm, E., Uin, J., Komsaare, K., Attoui, M. and Kulmala, M.: Results
10 of the first air ion spectrometer calibration and intercomparison workshop, *Atmos. Chem.*
11 *Phys.*, 9(1), 141–154, doi:10.5194/acp-9-141-2009, 2009.

12 Baars, H., Ansmann, A., Engelmann, R. and Althausen, D.: Continuous monitoring of the
13 boundary-layer top with lidar, *Atmos. Chem. Phys.*, 8, 7281–7296, 2008.

14 Birmili, W., Berresheim, H., Plass-Dülmer, C., Elste, T., Gilge, S., Wiedensohler, A. and
15 Uhrner, U.: The Hohenpeissenberg aerosol formation experiment (HAFEX): a long-term
16 study including size-resolved aerosol, H₂SO₄, OH, and monoterpenes measurements, *Atmos.*
17 *Chem. Phys.*, 3(2), 361–376, doi:10.5194/acp-3-361-2003, 2003.

18 Boulon, J., Sellegri, K., Hervo, M., Picard, D., Pichon, J.-M., Fréville, P. and Laj, P.:
19 Investigation of nucleation events vertical extent: a long term study at two different altitude
20 sites, *Atmos. Chem. Phys.*, 11(12), 5625–5639, doi:10.5194/acp-11-5625-2011, 2011.

21 Boulon, J., Sellegri, K., Venzac, H., Picard, D., Weingartner, E., Wehrle, G., Collaud Coen,
22 M., Bütikofer, R., Flückiger, E., Baltensperger, U. and Laj, P.: New particle formation and
23 ultrafine charged aerosol climatology at a high altitude site in the Alps (Jungfrauoch, 3580 m
24 a.s.l., Switzerland), *Atmos. Chem. Phys.*, 10(19), 9333–9349, doi:10.5194/acp-10-9333-2010,
25 2010.

26 Bourcier, L., Sellegri, K., Chausse, P., Pichon, J. M. and Laj, P.: Seasonal variation of water-
27 soluble inorganic components in aerosol size-segregated at the puy de Dôme station (1,465 m
28 a.s.l.), France, *J Atmos Chem*, 69(1), 47–66, doi:10.1007/s10874-012-9229-2, 2012.

1 Brooks, I. M.: Finding Boundary Layer Top: Application of a Wavelet Covariance Transform
2 to Lidar Backscatter Profiles, *Journal of Atmospheric and Oceanic Technology*, 20(8), 1092–
3 1105, doi:10.1175/1520-0426(2003)020<1092:FBLTAO>2.0.CO;2, 2003.

4 Clarke, A. D., Varner, J. L., Eisele, F., Mauldin, R. L., Tanner, D. and Litchy, M.: Particle
5 production in the remote marine atmosphere: Cloud outflow and subsidence during ACE 1,
6 *Journal of Geophysical Research: Atmospheres*, 103(D13), 16397–16409,
7 doi:10.1029/97JD02987, 1998.

8 Draxler, R. R. and Rolph, G. D.: HYSPLIT (Hybrid Single-Particle Lagrangian Integrated
9 Trajectory) Model access via NOAA ARL READY website
10 (<http://www.arl.noaa.gov/ready/hysplit4.html>), 2003.

11 Eisele, F. L.: Natural and anthropogenic negative ions in the troposphere, *Journal of*
12 *Geophysical Research: Atmospheres* (1984–2012), 94(D2), 2183–2196, 1989.

13 Freney, E. J., Sellegri, K., Canonaco, F., Boulon, J., Hervo, M., Weigel, R., Pichon, J. M.,
14 Colomb, A., Prévôt, A. S. H. and Laj, P.: Seasonal variations in aerosol particle composition
15 at the puy-de-Dôme research station in France, *Atmos. Chem. Phys.*, 11(24), 13047–13059,
16 doi:10.5194/acp-11-13047-2011, 2011.

17 Hamed, A., Korhonen, H., Sihto, S.-L., Joutsensaari, J., Järvinen, H., Petäjä, T., Arnold, F.,
18 Nieminen, T., Kulmala, M., Smith, J. N., Lehtinen, K. E. J. and Laaksonen, A.: The role of
19 relative humidity in continental new particle formation, *J. Geophys. Res.*, 116(D3), D03202,
20 doi:10.1029/2010JD014186, 2011.

21 Hari, P. and Kulmala, M.: Station for measuring ecosystem-atmosphere relations, *Boreal*
22 *Environ. Res*, 10, 315–322, 2005.

23 Hirsikko, A., Laakso, L., Horrak, U., Aalto, P. P., Kerminen, V. and Kulmala, M.: Annual and
24 size dependent variation of growth rates and ion concentrations in boreal forest, *Boreal*
25 *environment research*, 10(5), 357, 2005.

26 Hörrak, U., Aalto, P. P., Salm, J., Komsaare, K., Tammet, H., Mäkelä, J. M., Laakso, L. and
27 Kulmala, M.: Variation and balance of positive air ion concentrations in a boreal forest,
28 *Atmos. Chem. Phys.*, 8(3), 655–675, doi:10.5194/acp-8-655-2008, 2008.

1 Jeong, C.-H., Hopke, P. K., Chalupa, D. and Utell, M.: Characteristics of Nucleation and
2 Growth Events of Ultrafine Particles Measured in Rochester, NY, *Environ. Sci. Technol.*,
3 38(7), 1933–1940, doi:10.1021/es034811p, 2004.

4 Jokinen, T., Sipilä, M., Junninen, H., Ehn, M., Lönn, G., Hakala, J., Petäjä, T., Mauldin III, R.
5 L., Kulmala, M. and Worsnop, D. R.: Atmospheric sulphuric acid and neutral cluster
6 measurements using CI-APi-TOF, *Atmos. Chem. Phys.*, 12(9), 4117–4125, doi:10.5194/acp-
7 12-4117-2012, 2012.

8 Junninen, H., Ehn, M., Petäjä, T., Luosujärvi, L., Kotiaho, T., Kostianen, R., Rohner, U.,
9 Gonin, M., Fuhrer, K., Kulmala, M. and Worsnop, D. R.: A high-resolution mass
10 spectrometer to measure atmospheric ion composition, *Atmospheric Measurement*
11 *Techniques*, 3(4), 1039–1053, doi:10.5194/amt-3-1039-2010, 2010.

12 Kangasluoma, J., Junninen, H., Lehtipalo, K., Mikkilä, J., Vanhanen, J., Attoui, M., Sipilä,
13 M., Worsnop, D., Kulmala, M. and Petäjä, T.: Remarks on Ion Generation for CPC Detection
14 Efficiency Studies in Sub-3-nm Size Range, *Aerosol Science and Technology*, 47(5), 556–
15 563, doi:10.1080/02786826.2013.773393, 2013.

16 Kim, C. S., Okuyama, K. and de la Mora, J. F.: Performance evaluation of an improved
17 particle size magnifier (PSM) for single nanoparticle detection, *Aerosol Science &*
18 *Technology*, 37(10), 791–803, 2003.

19 Kirkby, J., Curtius, J., Almeida, J., Dunne, E., Duplissy, J., Ehrhart, S., Franchin, A., Gagné,
20 S., Ickes, L., Kürten, A., Kupc, A., Metzger, A., Riccobono, F., Rondo, L., Schobesberger, S.,
21 Tsagkogeorgas, G., Wimmer, D., Amorim, A., Bianchi, F., Breitenlechner, M., David, A.,
22 Dommen, J., Downard, A., Ehn, M., Flagan, R. C., Haider, S., Hansel, A., Hauser, D., Jud,
23 W., Junninen, H., Kreissl, F., Kvashin, A., Laaksonen, A., Lehtipalo, K., Lima, J., Lovejoy, E.
24 R., Makhmutov, V., Mathot, S., Mikkilä, J., Minginette, P., Mogo, S., Nieminen, T., Onnela,
25 A., Pereira, P., Petäjä, T., Schnitzhofer, R., Seinfeld, J. H., Sipilä, M., Stozhkov, Y.,
26 Stratmann, F., Tomé, A., Vanhanen, J., Viisanen, Y., Vrtala, A., Wagner, P. E., Walther, H.,
27 Weingartner, E., Wex, H., Winkler, P. M., Carslaw, K. S., Worsnop, D. R., Baltensperger, U.
28 and Kulmala, M.: Role of sulphuric acid, ammonia and galactic cosmic rays in atmospheric
29 aerosol nucleation, *Nature*, 476(7361), 429–433, doi:10.1038/nature10343, 2011.

30 Kontkanen, J., Lehtinen, K. E. J., Nieminen, T., Manninen, H. E., Lehtipalo, K., Kerminen,
31 V.-M. and Kulmala, M.: Estimating the contribution of ion–ion recombination to sub-2 nm

1 cluster concentrations from atmospheric measurements, *Atmos. Chem. Phys.*, 13(22), 11391–
2 11401, doi:10.5194/acp-13-11391-2013, 2013.

3 Kuang, C., Chen, M., McMurry, P. H. and Wang, J.: Modification of Laminar Flow Ultrafine
4 Condensation Particle Counters for the Enhanced Detection of 1 nm Condensation Nuclei,
5 *Aerosol Science and Technology*, 46(3), 309–315, 2012a.

6 Kuang, C., Chen, M., Zhao, J., Smith, J., McMurry, P. H. and Wang, J.: Size and time-
7 resolved growth rate measurements of 1 to 5 nm freshly formed atmospheric nuclei, *Atmos.*
8 *Chem. Phys.*, 12(7), 3573–3589, doi:10.5194/acp-12-3573-2012, 2012b.

9 Kulmala, M., Kontkanen, J., Junninen, H., Lehtipalo, K., Manninen, H. E., Nieminen, T.,
10 Petäjä, T., Sipilä, M., Schobesberger, S., Rantala, P., Franchin, A., Jokinen, T., Järvinen, E.,
11 Äijälä, M., Kangasluoma, J., Hakala, J., Aalto, P. P., Paasonen, P., Mikkilä, J., Vanhanen, J.,
12 Aalto, J., Hakola, H., Makkonen, U., Ruuskanen, T., Mauldin, R. L., Duplissy, J., Vehkamäki,
13 H., Bäck, J., Kortelainen, A., Riipinen, I., Kurtén, T., Johnston, M. V., Smith, J. N., Ehn, M.,
14 Mentel, T. F., Lehtinen, K. E. J., Laaksonen, A., Kerminen, V.-M. and Worsnop, D. R.:
15 Direct Observations of Atmospheric Aerosol Nucleation, *Science*, 339(6122), 943–946,
16 doi:10.1126/science.1227385, 2013.

17 Kulmala, M., Riipinen, I., Sipilä, M., Manninen, H. E., Petäjä, T., Junninen, H., Maso, M. D.,
18 Mordas, G., Mirme, A., Vana, M., Hirsikko, A., Laakso, L., Harrison, R. M., Hanson, I.,
19 Leung, C., Lehtinen, K. E. J. and Kerminen, V.-M.: Toward Direct Measurement of
20 Atmospheric Nucleation, *Science*, 318(5847), 89–92, doi:10.1126/science.1144124, 2007.

21 Kulmala, M., Vehkamäki, H., Petäjä, T., Dal Maso, M., Lauri, A., Kerminen, V.-M., Birmili,
22 W. and McMurry, P. H.: Formation and growth rates of ultrafine atmospheric particles: a
23 review of observations, *Journal of Aerosol Science*, 35(2), 143–176, 2004.

24 Lehtipalo, K., Kulmala, M., Sipilä, M., Petäjä, T., Vana, M., Ceburnis, D., Dupuy, R. and
25 O’Dowd, C.: Nanoparticles in boreal forest and coastal environment: a comparison of
26 observations and implications of the nucleation mechanism, *Atmos. Chem. Phys.*, 10(15),
27 7009–7016, doi:10.5194/acp-10-7009-2010, 2010.

28 Lehtipalo, K., Sipilä, M., Riipinen, I., Nieminen, T. and Kulmala, M.: Analysis of
29 atmospheric neutral and charged molecular clusters in boreal forest using pulse-height CPC,
30 *Atmos. Chem. Phys.*, 9(12), 4177–4184, doi:10.5194/acp-9-4177-2009, 2009.

1 Lihavainen, H., Komppula, M., Kerminen, V.-M., Järvinen, H., Viisanen, Y., Lehtinen, K.,
2 Vana, M. and Kulmala, M.: Size distributions of atmospheric ions inside clouds and in cloud-
3 free air at a remote continental site, *Boreal environment research*, 12(3), 337–344, 2007.

4 Makkonen, R., Asmi, A., Kerminen, V.-M., Boy, M., Arneth, A., Hari, P. and Kulmala, M.:
5 Air pollution control and decreasing new particle formation lead to strong climate warming,
6 *Atmos. Chem. Phys.*, 12(3), 1515–1524, doi:10.5194/acp-12-1515-2012, 2012.

7 Manninen, H. E., Franchin, A., Schobesberger, S., Hirsikko, A., Hakala, J., Skromulis, A.,
8 Kangasluoma, J., Ehn, M., Junninen, H. and Mirme, A.: Characterisation of corona-generated
9 ions used in a Neutral cluster and Air Ion Spectrometer (NAIS), *Atmos. Meas. Tech*, 4, 2767–
10 2776, 2011.

11 Manninen, H. E., Nieminen, T., Asmi, E., Gagné, S., Häkkinen, S., Lehtipalo, K., Aalto, P.,
12 Vana, M., Mirme, A., Mirme, S., Hörrak, U., Plass-Dülmer, C., Stange, G., Kiss, G., Hoffer,
13 A., Törő, N., Moerman, M., Henzing, B., de Leeuw, G., Brinkenberg, M., Kouvarakis, G. N.,
14 Bougiatioti, A., Mihalopoulos, N., O’Dowd, C., Ceburnis, D., Arneth, A., Svenningsson, B.,
15 Swietlicki, E., Tarozzi, L., Decesari, S., Facchini, M. C., Birmili, W., Sonntag, A.,
16 Wiedensohler, A., Boulon, J., Sellegri, K., Laj, P., Gysel, M., Bukowiecki, N., Weingartner,
17 E., Wehrle, G., Laaksonen, A., Hamed, A., Joutsensaari, J., Petäjä, T., Kerminen, V.-M. and
18 Kulmala, M.: EUCAARI ion spectrometer measurements at 12 European sites – analysis of
19 new particle formation events, *Atmos. Chem. Phys.*, 10(16), 7907–7927, doi:10.5194/acp-10-
20 7907-2010, 2010.

21 Manninen, H. E., Petäjä, T., Asmi, E., Riipinen, I., Nieminen, T., Mikkilä, J., Horrak, U.,
22 Mirme, A., Mirme, S. and Laakso, L.: Long-term field measurements of charged and neutral
23 clusters using Neutral cluster and Air Ion Spectrometer (NAIS), *Boreal Environ. Res*, 14,
24 591–605, 2009.

25 Merikanto, J., Spracklen, D. V., Mann, G. W., Pickering, S. J. and Carslaw, K. S.: Impact of
26 nucleation on global CCN, *Atmos. Chem. Phys.*, 9(21), 8601–8616, doi:10.5194/acp-9-8601-
27 2009, 2009.

28 Metzger, A., Verheggen, B., Dommen, J., Duplissy, J., Prevot, A. S. H., Weingartner, E.,
29 Riipinen, I., Kulmala, M., Spracklen, D. V., Carslaw, K. S. and Baltensperger, U.: Evidence
30 for the role of organics in aerosol particle formation under atmospheric conditions, *Proc Natl*
31 *Acad Sci U S A*, 107(15), 6646–6651, doi:10.1073/pnas.0911330107, 2010.

1 Mikkonen, S., Romakkaniemi, S., Smith, J. N., Korhonen, H., Petäjä, T., Plass-Duelmer, C.,
2 Boy, M., McMurry, P. H., Lehtinen, K. E. J., Joutsensaari, J., Hamed, A., Mauldin III, R. L.,
3 Birmili, W., Spindler, G., Arnold, F., Kulmala, M. and Laaksonen, A.: A statistical proxy for
4 sulphuric acid concentration, *Atmos. Chem. Phys.*, 11(21), 11319–11334, doi:10.5194/acp-
5 11-11319-2011, 2011.

6 Mirme, A., Tamm, E., Mordas, G., Vana, M., Uin, J., Mirme, S., Bernotas, T., Laakso, L.,
7 Hirsikko, A. and Kulmala, M.: A wide-range multi-channel Air Ion Spectrometer, *Boreal*
8 *environment research*, 12(3), 247–264, 2007.

9 Mirme, S. and Mirme, A.: The mathematical principles and design of the NAIS – a
10 spectrometer for the measurement of cluster ion and nanometer aerosol size distributions,
11 *Atmospheric Measurement Techniques*, 6(4), 1061–1071, doi:10.5194/amt-6-1061-2013,
12 2013.

13 Mirme, S., Mirme, A., Minikin, A., Petzold, A., Hörrak, U., Kerminen, V.-M. and Kulmala,
14 M.: Atmospheric sub-3 nm particles at high altitudes, *Atmos. Chem. Phys.*, 10(2), 437–451,
15 doi:10.5194/acp-10-437-2010, 2010.

16 Neitola, K., Asmi, E., Komppula, M., Hyvärinen, A.-P., Raatikainen, T., Panwar, T. S.,
17 Sharma, V. P. and Lihavainen, H.: New particle formation infrequently observed in
18 Himalayan foothills – why?, *Atmos. Chem. Phys.*, 11(16), 8447–8458, doi:10.5194/acp-11-
19 8447-2011, 2011.

20 Paasonen, P., Nieminen, T., Asmi, E., Manninen, H. E., Petäjä, T., Plass-Dülmer, C., Flentje,
21 H., Birmili, W., Wiedensohler, A., Hörrak, U., Metzger, A., Hamed, A., Laaksonen, A.,
22 Facchini, M. C., Kerminen, V.-M. and Kulmala, M.: On the roles of sulphuric acid and low-
23 volatility organic vapours in the initial steps of atmospheric new particle formation, *Atmos.*
24 *Chem. Phys.*, 10(22), 11223–11242, doi:10.5194/acp-10-11223-2010, 2010.

25 Petäjä, T., Mauldin III, R. L., Kosciuch, E., McGrath, J., Nieminen, T., Paasonen, P., Boy,
26 M., Adamov, A., Kotiaho, T. and Kulmala, M.: Sulfuric acid and OH concentrations in a
27 boreal forest site, *Atmos. Chem. Phys.*, 9(19), 7435–7448, doi:10.5194/acp-9-7435-2009,
28 2009.

29 Rose, C., Boulon, J., Hervo, M., Holmgren, H., Asmi, E., Ramonet, M., Laj, P. and Sellegri,
30 K.: Long-term observations of cluster ion concentration, sources and sinks in clear sky

1 conditions at the high-altitude site of the Puy de Dôme, France, *Atmos. Chem. Phys.*, 13(22),
2 11573–11594, doi:10.5194/acp-13-11573-2013, 2013.

3 Sihto, S.-L., Kulmala, M., Kerminen, V.-M., Dal Maso, M., Petäjä, T., Riipinen, I., Korhonen,
4 H., Arnold, F., Janson, R., Boy, M., Laaksonen, A. and Lehtinen, K. E. J.: Atmospheric
5 sulphuric acid and aerosol formation: implications from atmospheric measurements for
6 nucleation and early growth mechanisms, *Atmos. Chem. Phys.*, 6(12), 4079–4091,
7 doi:10.5194/acp-6-4079-2006, 2006.

8 Spracklen, D. V., Carslaw, K. S., Kulmala, M., Kerminen, V.-M., Sihto, S.-L., Riipinen, I.,
9 Merikanto, J., Mann, G. W., Chipperfield, M. P. and Wiedensohler, A.: Contribution of
10 particle formation to global cloud condensation nuclei concentrations, *Geophysical Research*
11 *Letters*, 35(6) [online] Available from:
12 <http://onlinelibrary.wiley.com/doi/10.1029/2007GL033038/full> (Accessed 17 October 2013),
13 2008.

14 Tammet, H. and Kulmala, M.: Simulation tool for atmospheric aerosol nucleation bursts,
15 *Journal of Aerosol Science*, 36(2), 173–196, doi:10.1016/j.jaerosci.2004.08.004, 2005.

16 Vanhanen, J., Mikkilä, J., Lehtipalo, K., Sipilä, M., Manninen, H. E., Siivola, E., Petäjä, T.
17 and Kulmala, M.: Particle Size Magnifier for Nano-CN Detection, *Aerosol Science and*
18 *Technology*, 45(4), 533–542, doi:10.1080/02786826.2010.547889, 2011.

19 Venzac, H., Sellegri, K. and Laj, P.: Nucleation events detected at the high altitude site of the
20 Puy de Dôme Research Station, France, *Boreal environment research*, 12(3), 345–359, 2007.

21 Venzac, H., Sellegri, K., Laj, P., Villani, P., Bonasoni, P., Marinoni, A., Cristofanelli, P.,
22 Calzolari, F., Fuzzi, S. and Decesari, S.: High frequency new particle formation in the
23 Himalayas, *Proceedings of the National Academy of Sciences*, 105(41), 15666–15671, 2008.

24 Venzac, H., Sellegri, K., Villani, P., Picard, D. and Laj, P.: Seasonal variation of aerosol size
25 distributions in the free troposphere and residual layer at the puy de Dôme station, France,
26 *Atmos. Chem. Phys.*, 9(4), 1465–1478, doi:10.5194/acp-9-1465-2009, 2009.

27 Wang, J. and Wexler, A. S.: Adsorption of organic molecules may explain growth of newly
28 nucleated clusters and new particle formation, *Geophysical Research Letters*, n/a–n/a,
29 doi:10.1002/grl.50455, 2013.

1 Wimmer, D., Lehtipalo, K., Franchin, A., Kangasluoma, J., Kreissl, F., Kürten, A., Kupc, A.,
2 Metzger, A., Mikkilä, J., Petäjä, T., Riccobono, F., Vanhanen, J., Kulmala, M. and Curtius, J.:
3 Performance of diethylene glycol-based particle counters in the sub-3 nm size range,
4 Atmospheric Measurement Techniques, 6(7), 1793–1804, doi:10.5194/amt-6-1793-2013,
5 2013.

6 Young, L.-H., Benson, D. R., Montanaro, W. M., Lee, S.-H., Pan, L. L., Rogers, D. C.,
7 Jensen, J., Stith, J. L., Davis, C. A., Campos, T. L., Bowman, K. P., Cooper, W. A. and Lait,
8 L. R.: Enhanced new particle formation observed in the northern midlatitude tropopause
9 region, J. Geophys. Res., 112(D10), D10218, doi:10.1029/2006JD008109, 2007.

10

11

12

13

14

15

16

17

18

19

20

21

22

23

24

25

26

1 Table 1. Cluster concentrations for each sub-period. Median, 25th and 75th percentiles of
 2 charged cluster concentration (N_i), total cluster concentration (N_{tot}) and neutral cluster
 3 concentration (N_n) during the different periods. The indices *day* refer to values calculated
 4 over the whole day whereas the indices *nucl* refer to values calculated during the time period
 5 10:30 – 14:00 (UTC). Indication <LDL refers to concentrations below the lower detection
 6 limit (500 cm⁻³) that was set for the total cluster concentration measured by the PSM;
 7 corresponding neutral cluster concentrations which are negative are not reported. The
 8 occurrence of NPF during the sub-periods is shown in the table. February 2012, puy de Dôme.

	Period 1			Period 2			Period 3		
		NPF			No NPF			NPF	
	Med.	25 th perc.	75 th perc.	Med.	25 th perc.	75 th perc.	Med.	25 th perc.	75 th perc
N_{i_day} (cm ⁻³)	275.0	187.6	391.9	651.5	563.3	690.0	752.3	681.3	802.8
N_{i_nucl} (cm ⁻³)	473.1	392.8	533.2	656.1	594.1	694.5	714.8	657.2	757.3
N_{tot_nucl} (cm ⁻³)	2049.1	821.9	7265.1	<LDL	<LDL	<LDL	921.4	715.8	1354.8
N_{n_nucl} (cm ⁻³)	2022.9	453.7	6765.0	-	-	-	281.4	7.4	854.0

9

10

11

12

13

1 Table 2. Summary of the particle formation event characteristics. $GR_{1.5-3}$ and GR_{3-5} are the
2 particle growth rates in 1.5-3 and 3-5 nm size ranges respectively, $J_{1.5}^{+/-}$ and $J_3^{+/-}$ are ion
3 formation rates at 1.5 and 3nm and $J_{1.5}^{tot}$ and J_3^{tot} are the corresponding total particle formation
4 rates during the event. Instruments used for the calculation of each parameter are specified in
5 the third row; for the NAIS also the mode used for the measurements is given. February 2012,
6 puy de Dôme.

7

Date	$GR_{1.5-3}$	GR_{3-5}	$J_{1.5}^+$	$J_{1.5}^-$	J_3^+	J_3^-	$J_{1.5}^{tot}$	J_3^{tot}
	(nm h ⁻¹)		(cm ⁻³ s ⁻¹)				(cm ⁻³ s ⁻¹)	
	NAIS		NAIS				PSM	NAIS
	<i>Ion</i>		<i>Ion</i>					<i>Particle</i>
02/10	1.65	8.45	0.084±0.057	0.025±0.033	0.049±0.044	0.062±0.050	2.87±3.71	1.38±0.91
02/11	1.93	3.58	-	0.010±0.030	-	0.013±0.009	0.58±0.64	0.34±0.23
02/12	14.36	15.57	0.468±0.083	0.311±0.100	0.139±0.071	0.245±0.147	18.24±10.11	2.20±0.94
02/28	1.90	-	0.183±0.067	0.022±0.027	-	-	0.42±0.28	-
02/29	10.45	5.06	0.686±0.148	0.132±0.070	0.011±0.011	0.011±0.012	4.32±2.84	0.60±0.58

8

9

10

11

12

13

14

15

16

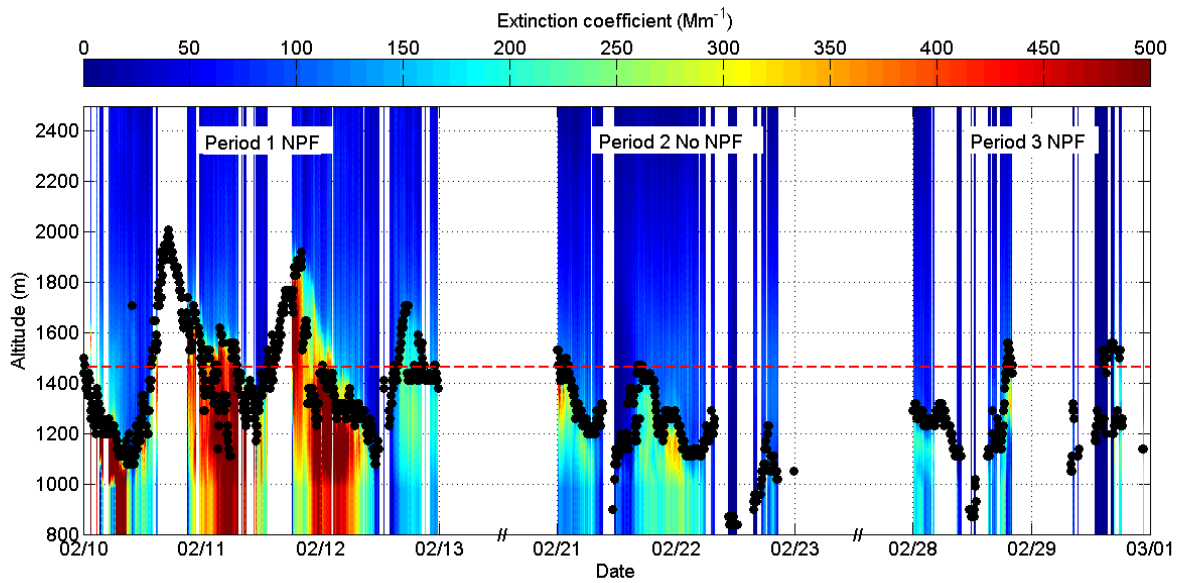
17

1
2
3
4
5
6
7
8
9
10
11
12
13
14
15
16
17

Table 3. Summary of the mean values of several atmospheric parameters for each sub - period. The occurrence of NPF during the sub-periods is indicated in the table. February 2012, puy de Dôme.

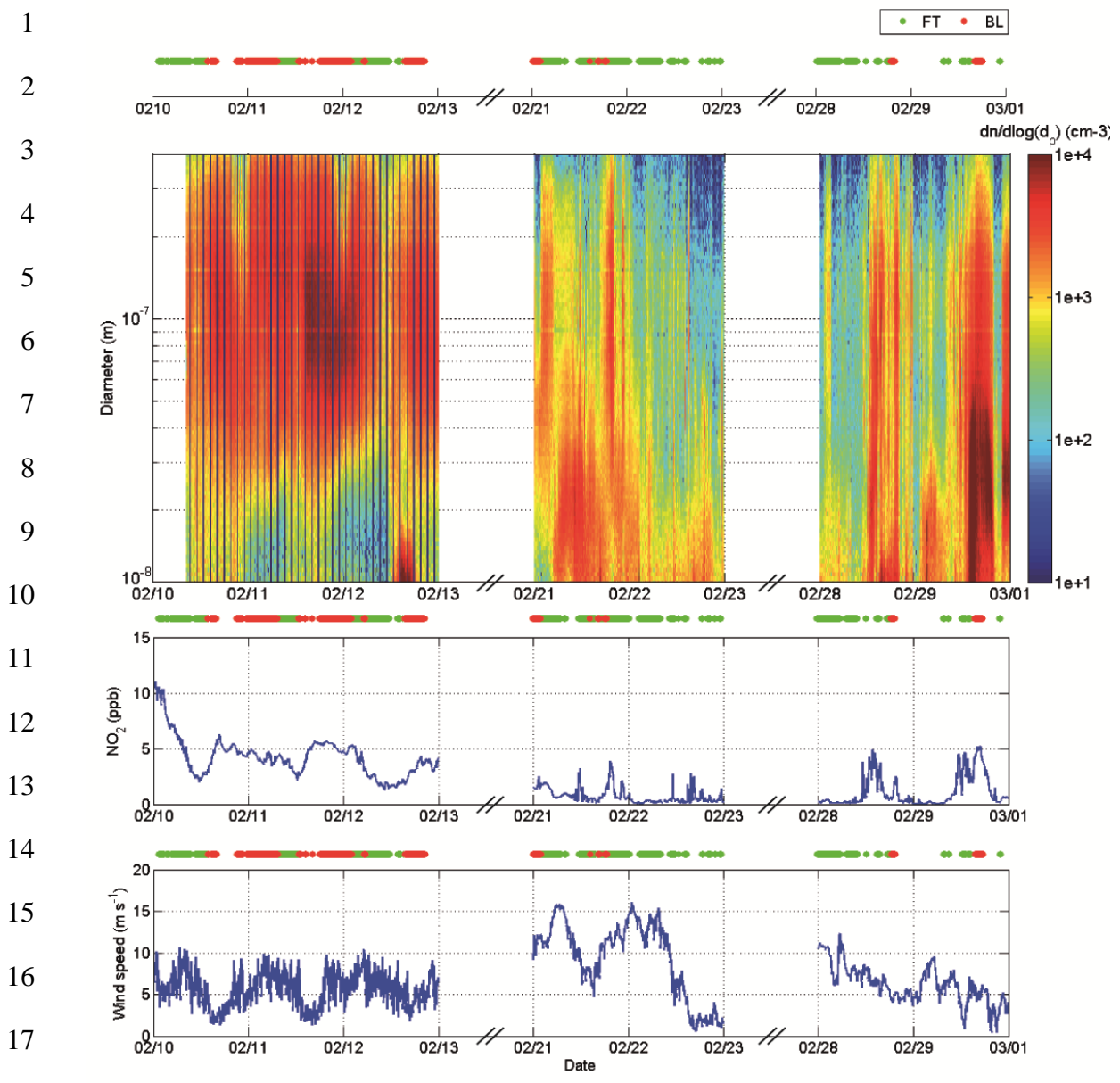
	Period 1	Period 2	Period 3
	NPF	No NPF	NPF
T (°C)	-14.24	-1.40	4.96
RH (%)	90.80	29.32	51.8
BC (ng m ⁻³)	687.53	87.83	<i>No data</i>
CS (s ⁻¹)	1.36 × 10 ⁻²	1.60 × 10 ⁻³	2.40 × 10 ⁻³
CO (ppb)	210.78	126.29	119.86
H ₂ SO ₄ (molec cm ⁻³)	0.72 × 10 ⁷	9.14 × 10 ⁷	2.79 × 10 ⁷

1
2



10 Fig. 1. Boundary layer height determination from LIDAR measurements. In the present
11 study, boundary layer (BL) height (black dots) is assumed to be equal to the aerosol mixing
12 layer height and was calculated using the WCT method. Red dashed line represents the
13 altitude of the station (1465 m a.s.l). The presence of high altitude clouds or frost on the
14 instrument avoids both the extinction coefficient and the BL height calculations. However,
15 when clouds are detected at the altitude of the station, the values of the extinction calculation
16 remain unreliable but a correct estimation of the BL height is allowed. The occurrence of NPF
17 during the sub-periods defined in Section 3.1 is indicated at the top of the figure. February
18 2012, puy de Dôme.

19
20
21
22
23



19 Fig. 2. SMPS particle size distribution, NO₂ concentrations and wind speed measurement
 20 used as additional information to distinguish between the BL and the FT.

21
 22
 23
 24
 25
 26

1
2
3
4
5
6
7
8
9
10
11
12
13
14
15
16
17
18
19
20
21
22
23
24
25
26

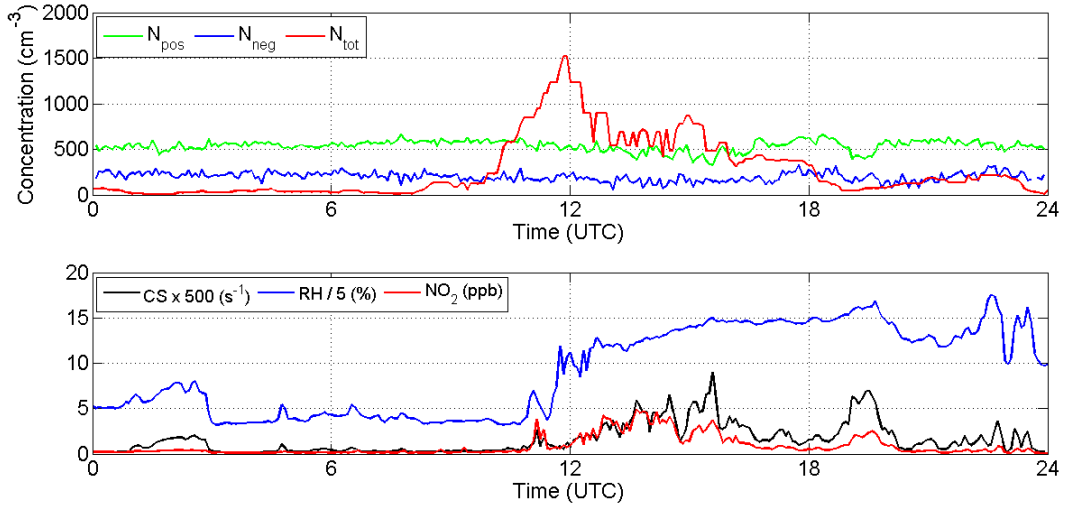


Fig. 3. Diurnal variation of the cluster concentrations (upper panel) and BL tracers (lower panel: condensation sink (CS), relative humidity (RH) and NO₂) observed at the PUY on the 28th of February.

1
2
3
4
5
6
7
8
9
10
11
12
13
14
15
16
17
18
19
20
21

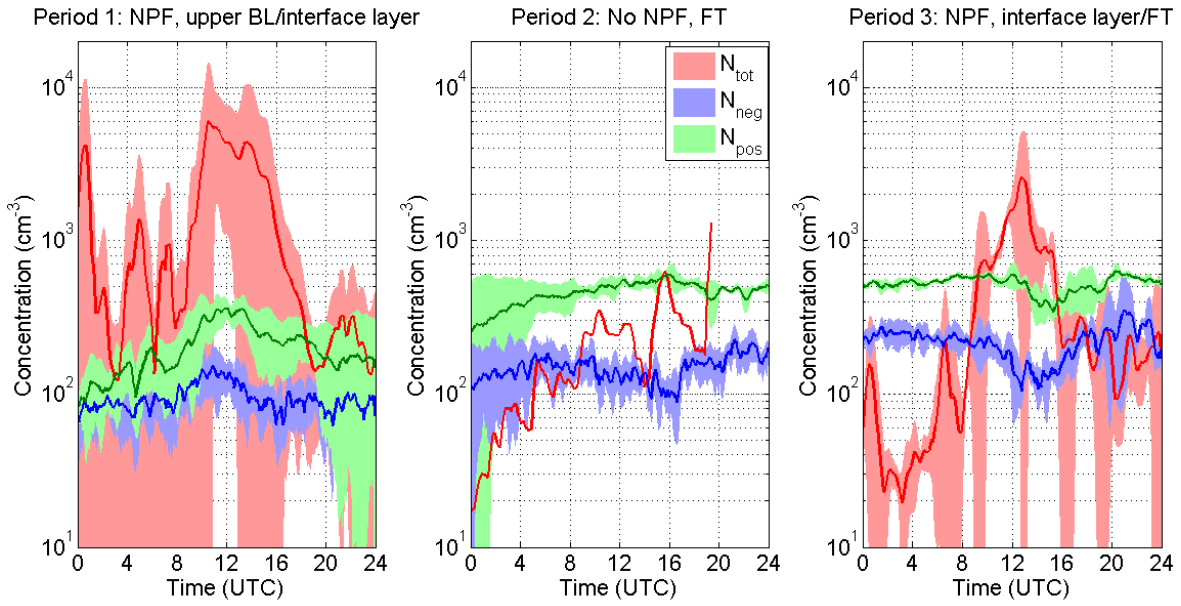


Fig. 4. Mean diurnal variation of positive (N_{pos}), negative (N_{neg}) and total (N_{tot}) clusters (1 to 2.5 nm mobility diameter) during the three sub-periods. Lower and upper limits of the shaded areas represent the standard deviation of the corresponding concentration. On non-event days, the lack in total cluster concentration measurement is due to an instrument failure. The occurrence of NPF during the sub-periods as well as the location of the station during nucleation hours are indicated at the top of the figure. February 2012, puy de Dôme..

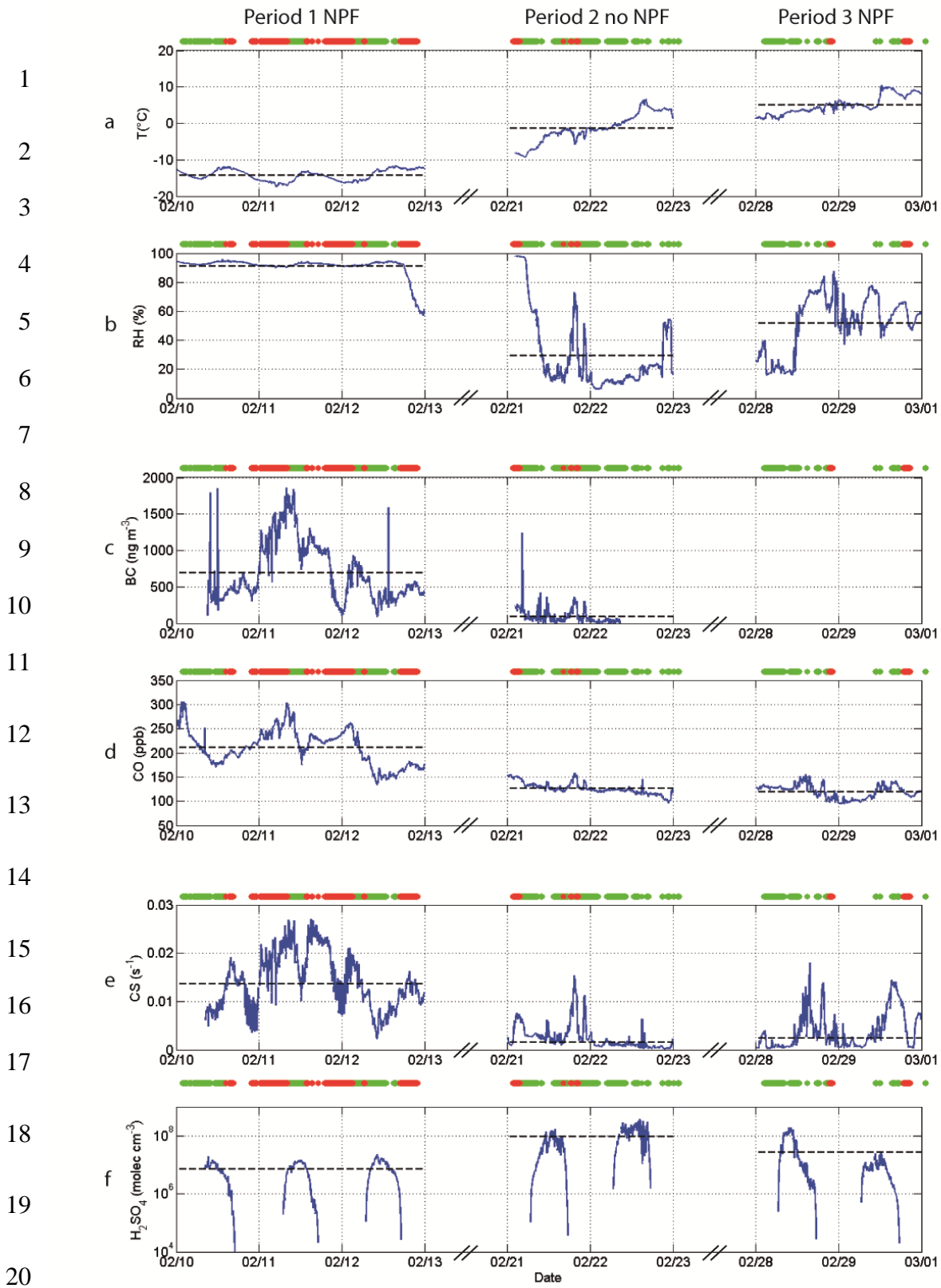
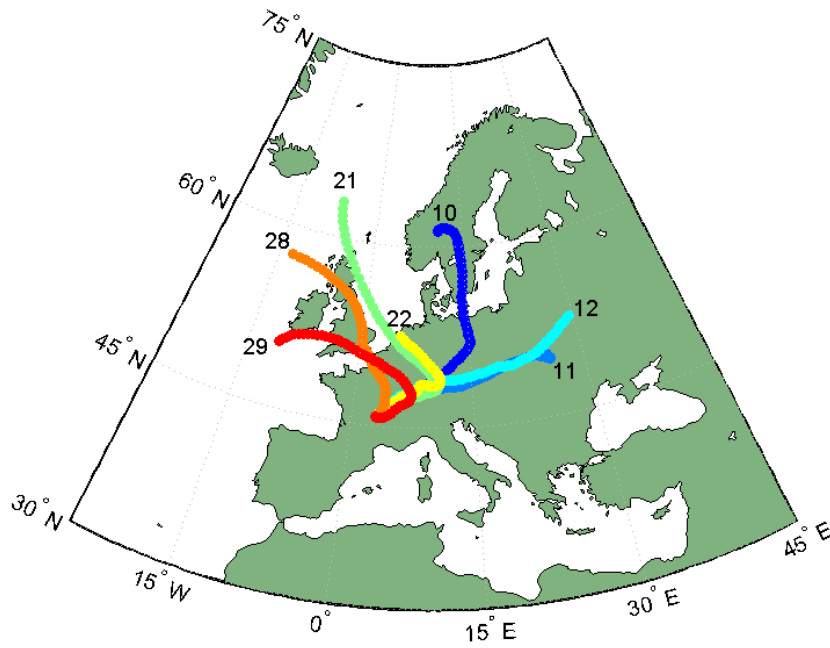


Fig. 5. Overview of atmospheric parameters during the studied period. Black dashed lines represent the mean value of each parameter during the three sub-periods. The occurrence of

1 NPF during the sub-periods as well as the location of the station in the BL (red) or in the FT
2 (green) are indicated at the top of the figure. February 2012, puy de Dôme.

3
4
5
6
7



17

18 Fig. 6. Three-days back trajectories of air masses reaching the puy de Dôme at 12:00 UTC.
19 Days are indicated on the map close to the corresponding trajectories.

20
21
22
23
24

1
2
3
4
5
6
7
8
9
10
11
12
13
14
15
16

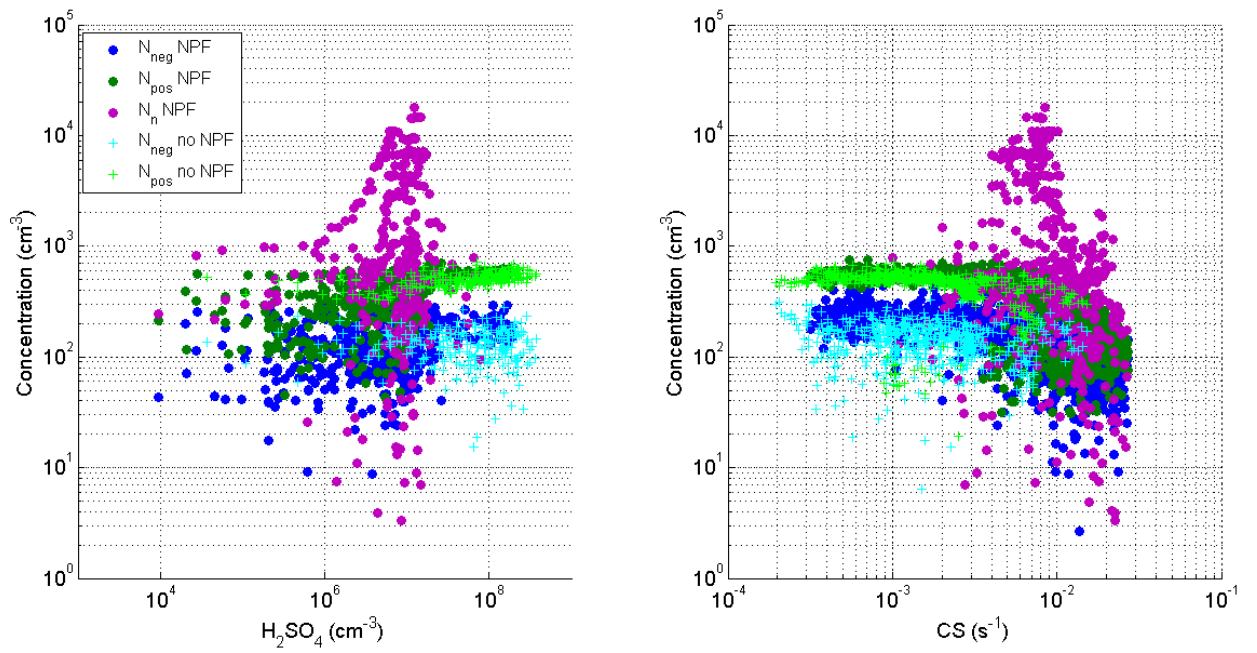


Fig. 7. Nanoparticle concentrations as a function of potential nucleation source and sink. Positive (N_{pos}), negative (N_{neg}) and neutral clusters (N_n) concentrations as a function of a) sulphuric acid concentration and b) condensation sink are reported separately, for NPF event and non-event days. Neutral cluster concentrations which are negative on non-event days are not shown on the figure. February 2012, puy de Dôme.